

# Determination of thermodynamic parameters for HIV DIS type loop–loop kissing complexes

Albert Weixlbaumer, Andreas Werner<sup>1</sup>, Christoph Flamm<sup>2</sup>, Eric Westhof<sup>1</sup>  
and Renée Schroeder\*

Max F. Perutz Laboratories, Department of Microbiology and Genetics, University of Vienna, Austria, <sup>1</sup>Institute of Molecular and Cellular Biology of the C.N.R.S., UPR9002, University Louis Pasteur, Strasbourg, France and <sup>2</sup>Department of Theoretical Chemistry and Structural Biology, University of Vienna, Austria

Received as resubmission August 1, 2004; Revised and Accepted September 3, 2004

## ABSTRACT

The HIV-1 type dimerization initiation signal (DIS) loop was used as a starting point for the analysis of the stability of Watson–Crick (WC) base pairs in a tertiary structure context. We used ultraviolet melting to determine thermodynamic parameters for loop–loop tertiary interactions and compared them with regular secondary structure RNA helices of the same sequences. In 1 M Na<sup>+</sup> the loop–loop interaction of a HIV-1 DIS type pairing is 4 kcal/mol more stable than its sequence in an equivalent regular and isolated RNA helix. This difference is constant and sequence independent, suggesting that the rules governing the stability of WC base pairs in the secondary structure context are also valid for WC base pairs in the tertiary structure context. Moreover, the effect of ion concentration on the stability of loop–loop tertiary interactions differs considerably from that of regular RNA helices. The stabilization by Na<sup>+</sup> and Mg<sup>2+</sup> is significantly greater if the base pairing occurs within the context of a loop–loop interaction. The dependence of the structural stability on salt concentration was defined via the slope of a  $T_m/\log[\text{ion}]$  plot. The short base-paired helices are stabilized by 8°C/log [Mg<sup>2+</sup>] or 11°C/log [Na<sup>+</sup>], whereas base-paired helices forming tertiary loop–loop interactions are stabilized by 16°C/log [Mg<sup>2+</sup>] and 26°C/log [Na<sup>+</sup>]. The different dependence on ionic strength that is observed might reflect the contribution of specific divalent ion binding to the preformation of the hairpin loops poised for the tertiary kissing loop–loop contacts.

## INTRODUCTION

RNAs are synthesized as single-stranded molecules and they need to fold into complex tertiary structures to reach their native functional states. RNA folding is dominated by intramolecular Watson–Crick (WC) base pairs, which form regular A-type helices defining the secondary structure. Two levels of

folding are observed, whereby the secondary structure helices form rapidly, followed by the more complex tertiary interactions building the 3D structure (1–6). Thermodynamic parameters describe the stability of nucleic acid molecules and the energies that control their structures. The method of choice for determination of RNA structure stability is thermal melting monitored by ultraviolet (UV) spectroscopy (7–12).

Tertiary structure is the outcome of interactions between secondary structure elements that are the basic building blocks of RNA structure. Little information is available on the energies that control interactions between tertiary structure elements. In general, energies that are involved in tertiary structure formation are lower than those involved in the formation of secondary structure (5). According to Leontis and Westhof (13), there are three categories of tertiary structure motifs: interactions between two double-stranded helices, between a helix and a single strand and between two single-stranded regions. Among the RNA motifs important for tertiary structure formation, WC base pairing is quite prevalent between two single-stranded regions, e.g. complementary hairpin loops forming loop–loop interactions. In large, intramolecular RNA systems like the ribosomal RNAs and group I introns, such intramolecular interactions are equivalent to pseudoknot formation. However, when such contacts occur intermolecularly between two RNAs, it is better to call them loop–loop motifs.

Intermolecular loop–loop interactions constitute a widely distributed three-dimensional motif and serve a diverse range of biological functions. Due to the increased accessibility of the bases in hairpin loops, intermolecular loop–loop interactions are particularly well adapted to trigger molecular recognition and to induce RNA–RNA annealing. Well known examples for loop–loop complexes, also called kissing loops, are the interaction between the CopA and CopTRNAs, between RNA I and RNA II, which regulate plasmid replication and the interaction between two self-complementary dimerization initiation signal (DIS) loops responsible for the dimerization of the genomic HIV RNA (14–16). The kissing complex between two DIS loops is the initial contact that precedes a refolding process, whereby the hairpin stems are opened to form an extended duplex between two HIV genomes (17–19).

The formation of stably folded structures requires the compensation of the negative charges of backbone phosphates,

\*To whom correspondence should be addressed. Tel: +43 1 4277 54690; Fax: +43 1 4277 9546; Email: renee.schroeder@univie.ac.at

whose electrostatic repulsion inhibits close packing. Two effects have to be taken into account (20): first, the increase in ionic strength of the bulk solution favors the formation of the species with the higher charge density, i.e. the more compactly folded RNA; second, structured RNAs provide specific binding pockets to coordinate divalent  $Mg^{2+}$  ions via outer- or inner-sphere binding, where partial dehydration of the metal ion may be required. Both effects contribute to compaction and folding of RNAs as a function of ion concentration, which can be monitored by UV melting (21). Tertiary structure formation of large RNA molecules is strongly dependent on the presence of divalent metal ions, preferentially  $Mg^{2+}$ . The UV melting experiments of highly structured RNAs, such as self-splicing group I introns, displayed strong structural stabilization with increasing  $Mg^{2+}$  concentrations (22–24).

In this paper we have analyzed the thermodynamic stability of loop–loop interactions derived from the HIV-1 DIS loop, addressing the following questions: (i) Is there a difference in stability between WC base pairs in a secondary structure context compared with WC base pairs in a tertiary structure context? (ii) Does the nearest neighbor model pertain to the approximate description of the loop–loop interaction? (iii) What is the contribution of the metal ions ( $Na^+$  and  $Mg^{2+}$ ) to the stability of loop–loop interactions compared with that of RNA duplexes of the same sequence?

## MATERIALS AND METHODS

### RNAs

The RNA oligomers were synthesized by either Eurogentec or Dharmacon. The oligomers were deprotected using the procedures specified by the manufacturer and were purified by gel electrophoresis. The RNA was stored at  $-20^{\circ}C$  in water. The measured sequences were the following: each set of complementary hairpin pair contained as stem 1, the sequence 5'-GGGCCGAANNNNNNACGGCCC-3' and as stem 2, 5'-CCCGGCAANNNNNNAGCCGGG-3'. The complementary loop sequences, depicted as N in Figure 1A, were 5'-CCUGCC-3' and 5'-GGCAGG-3'; 5'-CCGACC-3' and 5'-GGUCGG-3'; 5'-GAGAGG-3' and 5'-CCUCUC-3' and finally 5'-CUAAAC-3' and 5'-GUUUAG-3'.

### UV spectra

The UV melting experiments were performed in 10 mM cacodylic acid (pH 6.8). If not otherwise stated, the final monovalent salt concentration of this buffer was 18 mM  $Na^+$ , due to the addition of NaOH for pH adjustment. The final ionic conditions are indicated for each experiment. Up to six consecutive runs, successive heating and cooling profiles were recorded to detect possible hysteresis. Thermodynamic parameters were measured in 1 M  $Na^+$  final concentration without  $Mg^{2+}$ . The oligoribonucleotide single-strand concentrations were determined either by high temperature absorbance measurements ( $>80^{\circ}C$ ) or by alkaline hydrolysis (pH was adjusted afterwards) and absorbance measurements. All solutions were degassed prior to usage. The single strands forming hairpins were prepared separately, denatured for at least 10 min at  $90^{\circ}C$  at low salt, slowly chilled to room temperature and mixed in a 1:1 ratio with its complementary

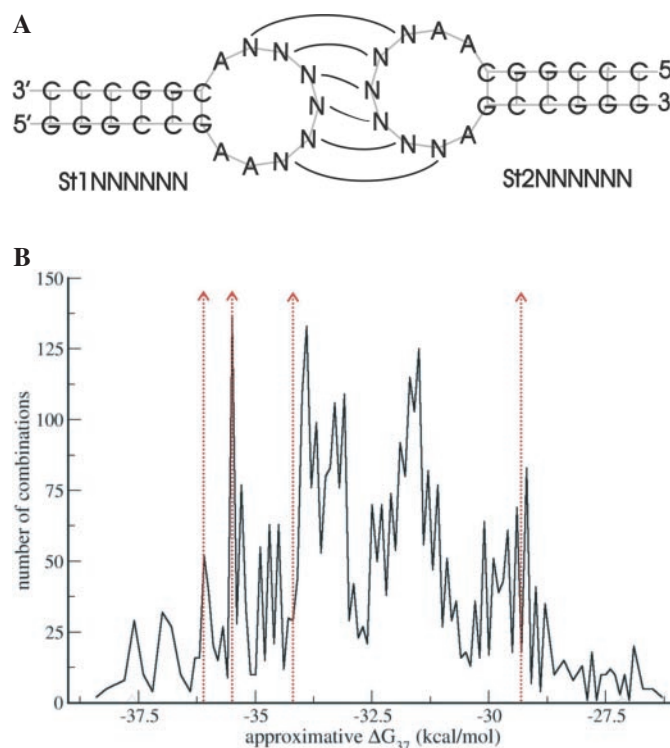


**Figure 1.** (A) Schematic representation of the hairpins derived from the HIV-1 DIS hairpin loop used in this study. The kissing loop complex between two hairpins is shown. The loop is composed of nine bases, whereby the six central bases participate in base pairing and are flanked by two adenines on the 5' side and one adenine on the 3' side. St1 and St2 stands for stem 1 or stem 2 including flanking adenines, N equals any of the four bases. (B) Abundance of sequences with distinct energy contributions to the kissing complex stability. Red arrows indicate positions of chosen sequences within the energy spectrum. Note that only a few sequences are very stable or very unstable due to the small number of possible CG or AU combinations.

counterpart. Absorbance versus temperature melting curves were measured at 260 nm with a heating (cooling) rate of  $0.5^{\circ}C/min$  either on a UVKON XL with a Biotek Thermo-system or on a Cary 100 Bio Varian Spectrophotometer.

### Calculation of thermodynamic parameters

Several methods exist for extracting thermodynamic parameters from UV melting curves (25). The main problem is the evaluation of the fraction of base-paired molecules. Instead of attempting to fit lower and higher temperature base lines, which would be error-prone due to the presence of the secondary and tertiary transitions, we determined melting transitions by calculating the second derivative of the absorbance versus temperature curve (curves were smoothed with a least square fit of second order polynomials) and successive determination of the null. The latter method introduces systematic errors in the derived  $T_m$  values. In order to evaluate these errors, we have tested a nonlinear fitting method of the absorbance curves to derive the  $T_m$  values and the thermodynamic parameters (see Supplementary Material). As expected, the  $T_m$  values are systematically underestimated by about  $2^{\circ}C$ , which translates, for the loop–loop interactions, into very small differences in  $\Delta G$  of 0.5 kcal/mol and  $\Delta S$  of 2 cal/mol/K.

Thermodynamic parameters for complex formation were derived by van't Hoff analysis (8).

$$\frac{R}{\Delta H^\circ} \cdot \ln\left(\frac{C_T}{4}\right) + \frac{\Delta S^\circ}{\Delta H^\circ} = \frac{1}{T_m}$$

The reciprocal melting temperature was plotted versus  $\ln(C_T/4)$ .  $C_T$  is the total strand concentration.

## RESULTS

### Design of RNA hairpins suitable for equilibrium melting experiments

We used the HIV-1 type DIS loop as a starting point for the measurement of the influence of tertiary structure on the thermal stability of WC base pairings. The DIS loop is a hairpin structure that contains a six-nucleotide self-complementary loop sequence preceded and followed by two and one adenines, respectively (Figure 1A). The original HIV DIS hairpin had to be redesigned in order to be able to derive sequence specific effects. Using the Vienna RNA package (26), sequences were designed where the six nucleotides involved in the kissing interaction were permuted to generate all possible combinations ( $4^6 = 4096$ ) and where the different stem sequences contained only GC pairs. The following criteria were used for choosing the sequence of the hairpins to be analyzed: (i) high thermal stability of the hairpin itself for a clear differentiation of the hairpin and loop-loop melting transitions, (ii) a small number of alternative suboptimal structures to assure that the vast majority of molecules in the thermodynamic ensemble adopts the hairpin fold, (iii) no self-complementary loop sequences in order to avoid homodimerization and as a consequence, extended duplex formation, (iv) inverted stems to avoid extended duplex formation and lastly (v) the 5' and 3' flanking adenines were retained. The obtained list of sequences was then combined with different stem sequences and folded *in silico*. The approximate free energies of kissing complex formation were generated by assuming that the nearest neighbor model is applicable. Figure 1B shows the abundance of sequences with distinct energies. The number of sequence combinations was plotted versus the approximate free energy of complex formation including the energy of hairpin formation.

As internal controls for the UV measurements and for the extraction method of the thermodynamic parameters from the experimental data, regular duplexes with sequences identical to those formed in the tertiary loop-loop interaction were measured and calculated.

### UV melting profiles of loop-loop interactions and their corresponding helices

The UV melting experiments were performed at 1 M NaCl to enable comparison of our data with published data and to allow calculation of expected stabilities with the available programs. A representative melting profile for the complementary loop sequences 5'-AACCGACCA-3' in stem 1 and 5'-AAGGUCGGA-3' in stem 2 is shown in Figure 2A. The consecutive recording of two heating and two cooling profiles indicates that no hysteresis occurs in the presence of monovalent ions. The first derivative of the melting profiles at

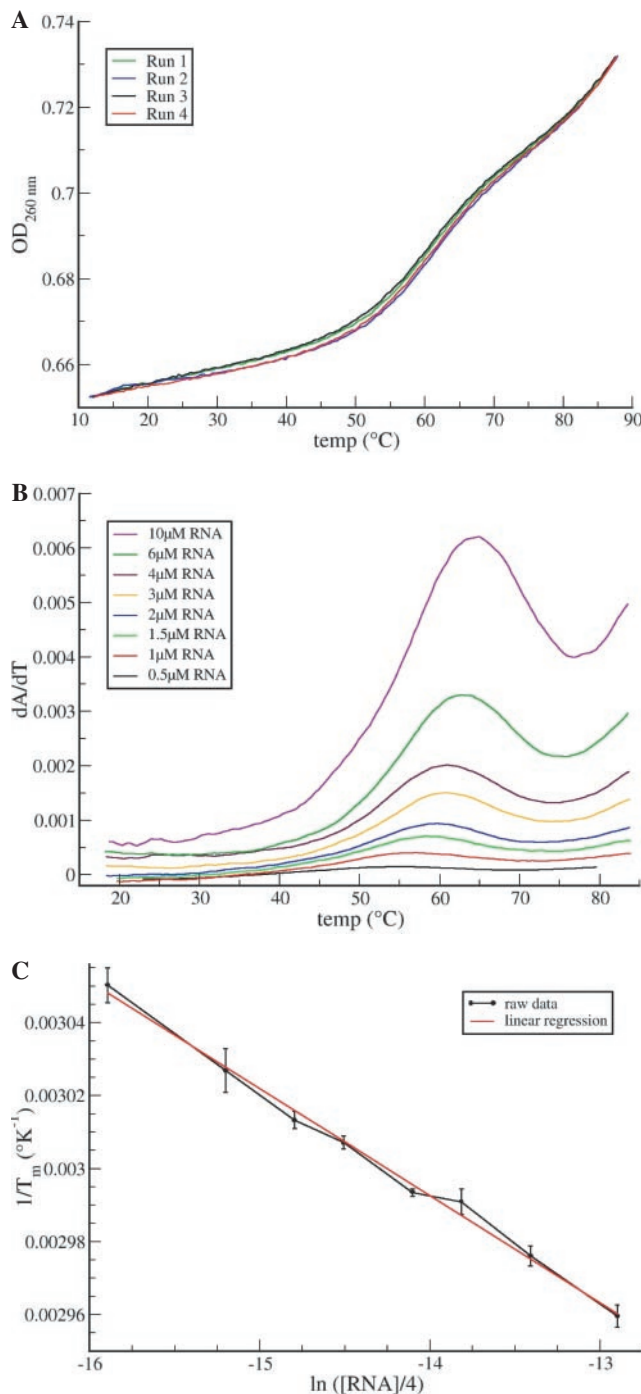


**Figure 2.** (A) Superimposed melting curves of St1CCGACC and St2GGUCGG complexes. The absorption versus temperature plots for two heating and two cooling runs are displayed. (B) Superimposed first derivatives of the melting curves of St1CCGACC and St2GGUCGG at different RNA concentrations indicated in the indented plot. (C) Van't Hoff analysis of melting curves of hairpins St1CCGACC and St2GGUCGG.

different RNA concentrations was superimposed and plotted versus temperature (Figure 2B). Two transitions are observed, an RNA concentration-dependent transition that shifts from 55° to 65°C and a second RNA concentration-independent transition that occurs above 85°C. In control melting experiments at low salt (18 mM Na<sup>+</sup>), where the hairpins were

melted separately in a monomeric reaction, only one concentration-independent transition at high temperature is detected, corresponding to the melting of the stems. Further control experiments with both hairpins at low salt concentration clearly allowed the detection of two transitions: the low temperature, concentration-dependent transition corresponding to the melting of the kissing loop and the high temperature, concentration-independent transition corresponding to the melting of the stems (data not shown). Therefore, we are confident that the low temperature transition corresponds to the bimolecular reaction representing the melting of the kissing complex.

The thermodynamic parameters were derived from van't Hoff plots as described in the materials and methods section. A representative plot is shown in Figure 2C. The  $1/T_m$  is linearly dependent on  $\ln(C_T/4)$ , where  $C_T$  represents the total RNA concentration. Table 1 indicates the measured parameters of four different pairs of complementary hairpins compared with the predicted values for regular RNA duplexes as calculated with the Vienna RNA package. As shown in Table 1, at 1 M  $\text{Na}^+$  concentration, the kissing complexes are more stable than the equivalent regular helices by a constant difference,  $\Delta\Delta G_{37}$ , of approximately  $-4.2$  kcal/mol independent of the loop sequence. When the thermodynamic values are compared to equivalent regular helices flanked by dangling adenines, the stability of the loop-loop helices is slightly more stable than the regular helices by  $\sim\Delta\Delta G_{37} = -1$  kcal/mol. Since we observe a constant difference in free energy of the kissing complex compared with regular duplexes, we conclude that the rules governing WC base pairing in secondary structure are also valid in tertiary structure, at least in the presence of 1 M  $\text{Na}^+$  ions and for this type of loop-loop interaction. We may assume that the nearest neighbor model could be used, in principle, to predict the stability of a WC base pair in tertiary interactions.

We not only calculated the stabilities of regular RNA helices but also measured the thermodynamic parameters for duplexes equivalent to the corresponding loop sequences in order to evaluate the quality and reliability of our measurements. We also wanted to compare the loop-loop complex parameters with measured values instead of predicted values. Table 2 shows the measured parameters for short oligos and

compares the free energy of duplex formation with that of the kissing complex formation. Again, as for the comparison with predicted values, the kissing complex is more stable by  $\sim\Delta\Delta G_{37} = -4.2$  kcal/mol when compared with duplexes without dangling adenines and  $\Delta\Delta G_{37} = -1.2$  kcal/mol for duplexes with dangling adenines. To evaluate further the reliability of our measurements, we compared our measured parameters for the oligos with predicted values calculated with the Vienna RNA package (Table 3). As can be seen, the differences are small, ranging from 0.17 to 0.57 kcal/mol and well within the thermal noise (10).

### Influence of ionic strength on the stability of the kissing loop

The stability of nucleic acid structure is strongly dependent on the ionic strength of the surrounding solution. We therefore measured the influence of monovalent and divalent ion concentration on the thermal stability of the loop-loop interaction. The UV melting experiments were performed as described in the material and methods section at different  $\text{Na}^+$  and  $\text{Mg}^{2+}$  concentrations. Figure 3 shows representative derivatives of the melting curves at different magnesium concentrations. As can be seen,  $\text{Mg}^{2+}$  greatly influences the thermal stability of the kissing complex reflected in the shift of the maxima towards higher temperatures with increasing  $\text{Mg}^{2+}$  concentrations. The  $T_m$  values increase from  $29^\circ\text{C}$  at  $1\ \mu\text{M}$   $\text{Mg}^{2+}$  to  $62^\circ\text{C}$  at  $5\ \text{mM}$   $\text{Mg}^{2+}$  (Figure 4). It should be noted that (i) at higher  $\text{Mg}^{2+}$  concentrations, the decay of the RNA becomes significant and therefore,  $T_m$  values are error-prone and (ii) in all experiments  $18\ \text{mM}$   $\text{Na}^+$  are present due to the sodium cacodylate buffer.

We further measured the effect of  $\text{Na}^+$  on the stability of the kissing complex by monitoring melting profiles at increasing  $[\text{Na}^+]$  from  $18\ \text{mM}$  to  $2\ \text{M}$   $\text{Na}^+$ . We compared the susceptibility of the kissing complex with the nature of the ion by plotting the  $T_m$  values versus the logarithm of ion concentration ( $T_m/\log[\text{ion}]$ , see Figure 4). For the kissing complex, the same  $T_m$  is obtained by adding either  $1\ \text{mM}$   $\text{Mg}^{2+}$  (against a background of  $18\ \text{mM}$  monovalent ions), or  $2\ \text{M}$   $\text{Na}^+$ . Both  $T_m/\log[\text{ion}]$  plots are sigmoid with maximal slopes of  $\sim 16^\circ$  and  $26^\circ\text{C}/\log[\text{ion}]$  for  $\text{Mg}^{2+}$  and for  $\text{Na}^+$ , respectively (Table 4).

**Table 1.** The thermodynamic parameters for the four hairpin pairs forming a kissing complex are shown. The  $T_m$  is shown for a total RNA concentration of  $10^{-5}\ \text{M}$

Complementary loop sequence	$\text{Na}^+$ conc. (mM)	$T_m$ ( $^\circ\text{C}$ ) (for $10^{-5}\ \text{M}$ RNA conc.)	$\Delta T_m$ ( $^\circ\text{C}$ )	$-\Delta H_{\text{app}}$ (kcal/mol)	$-\Delta S_{\text{app}}$ (cal/mol)	$-\Delta G_{37\text{app}}$ (kcal/mol)	$-\Delta\Delta G_{37}^{\text{a}}$ (kcal/mol)	$-\Delta\Delta G_{37}^{\text{b}}$ (kcal/mol)
CCUGCC GGACGG	1000	$67.3 \pm 0.4$	<b>19.0</b>	$75.7 \pm 1.2$	$196.6 \pm 0.5$	14.72	<b>-4.62</b>	<b>-1.12</b>
CCGACC GGCUGG	1000	$64.7 \pm 0.4$	<b>19.8</b>	$68.0 \pm 2.2$	$175.8 \pm 0.9$	13.48	<b>-3.98</b>	<b>-0.48</b>
GAGAGG CUCUCC	1000	$57.0 \pm 0.3$	<b>19.5</b>	$71.7 \pm 1.6$	$191.6 \pm 0.6$	12.28	<b>-4.08</b>	<b>-0.58</b>
CUAAAC GAUUUG	1000	$32.0 \pm 0.3$	<b>30.9</b>	$35.3 \pm 2.2$	$89.8 \pm 1.8$	7.45	<b>-4.15</b>	<b>-0.65</b>
						<b>mean:</b>	<b>-4.21</b>	<b>-0.71</b>

The  $\Delta T_m$  shows the differences between the measured melting temperatures and the predicted  $T_m$  for regular RNA duplexes with identical sequence and without dangling adenines. The two columns on the right show the differences in free energy compared to duplexes without dangling adenines (a) and with dangling adenines (b). In both cases, the free energy of the kissing complex is lower than for the corresponding RNA duplexes, indicating that at  $1\ \text{M}$   $\text{Na}^+$ , the kissing complex is more stable.

**Table 2.** Measured thermodynamic parameters for short oligoribonucleotide duplexes with and without dangling adenines

Complementary sequence	Na <sup>+</sup> conc. (mM)	$T_m$ (°C) ( $9 \times 10^{-6}$ M RNA)	$-\Delta H_{app}$ (kcal/mol)	$-\Delta S_{app}$ (cal/mol)	$-\Delta G_{37app}$ (kcal/mol)	$-\Delta\Delta G_{37}$ (kcal/mol)
ACCUGCC AGGACGGA	1000	61.6 ± 0.3	68.1 ± 0.3	177.6 ± 0.1	13.03	<b>1.69</b>
ACCGACCA AGGCUGGA	1000	58.6 ± 0.3	70.5 ± 0.9	186.6 ± 0.4	12.62	<b>0.86</b>
AGAGAGGA ACUCUCCA	1000	53.5 ± 0.3	62.3 ± 1.6	165.0 ± 0.7	11.16	<b>1.12</b>
ACUAAACA AGAUUUGA	1000	26.9 ± 0.1	49.6 ± 0.4	139.5 ± 0.2	6.34	<b>1.11</b>
CCUGCC GGACGG	1000	48.4 ± 0.3	63.90 ± 1.2	172.93 ± 0.5	10.27	<b>4.45</b>
CCGACC GGCUGG	1000	43.3 ± 0.4	59.2 ± 0.5	161.1 ± 0.2	9.21	<b>4.27</b>
GAGAGG CUCUCC	1000	40.0 ± 0.4	58.30 ± 2.3	160.56 ± 1.1	8.50	<b>3.78</b>
CUAAAC GAUUUG	1000	nc	—	—	—	—

The differences in free energy between the measured kissing loops and short duplexes are indicated in the right column in bold; nc indicates that this sequence does not form a complex at temperatures that can be monitored.

**Table 3.** Predicted thermodynamic parameters for short oligoribonucleotide duplexes are indicated and compared with measured parameters of identical sequences

Sequence	Predicted for duplex $-\Delta H$ (kcal/mol)	$-\Delta S$ (cal/mol)	$-\Delta G_{37}$ (kcal/mol)	$T_m$ Duplex (°C)	Predicted value–measured value <sup>b</sup>			
					$\Delta T_m$ (°C)	$-\Delta\Delta H$ (kcal/mol)	$-\Delta\Delta S$ (cal/mol)	$-\Delta\Delta G_{37}$ (kcal/mol)
ACCUGCC AGGACGGA	79.4	212.04	13.6	60.6	−1	−11.3	−34.44	<b>−0.57</b>
ACCGACCA AGGCUGGA	77.99	209.46	13.0	58.3	−0.3	−7.49	−22.86	<b>−0.38</b>
AGAGAGGA ACUCUCCA	75.99	207.21	11.7	52.9	−0.6	−13.69	−42.21	<b>−0.54</b>
ACUAAACA AGAUUUGA	59.99	171.42	6.8	31.0	4.1	−10.39	−31.92	<b>−0.46</b>
CCUGCC GGACGG	59.00	157.6	10.1	48.5	0.1	4.9	15.33	<b>0.17</b>
CCGACC GGCUGG	57.6	155.0	9.5	45.4	2.1	1.6	6.1	<b>−0.29</b>
GAGAGG CUCUCC	55.6	152.7	8.2	38.3	−1.7	2.7	7.86	<b>0.3</b>
CUAAAC <sup>a</sup> GAUUUG	26.0	73.1	3.3	< 0	—	—	—	—

Differences in free energies are indicated in right column in bold. Note that measurements of the duplex containing four AU base pairs were not possible due to the low  $T_m$  of the helix.

### Influence of ionic strength on the stability of regular RNA duplexes

To allow a comparison of our data on WC-helices in context of the loop–loop interaction, we measured the same oligo sequence with dangling adenines in the context of a regular RNA duplex at varying magnesium and sodium concentrations (Table 4 and Figure 4). The duplex is stabilized from a  $T_m$  of 39.9° to 58.9°C (Figure 4). Sodium stabilizes the regular helix from 44°C at 18 mM to 59°C at 2 M NaCl. As for the kissing complex, more sodium than magnesium is required in order to

reach comparable stabilities. The same  $T_m$  is obtained by adding 1 mM Mg<sup>2+</sup> or 0.8 M Na<sup>+</sup>. The  $T_m/\log$  [ion] plots for magnesium and sodium are shown in Figure 4, as green and blue curves.

### Increasing ionic strength stabilizes WC helices more efficiently in the context of loop–loop interaction than within regular duplexes

At low ionic concentrations, the kissing loop melts before the regular helix: the  $T_m$  of the kissing complex at 1 μM

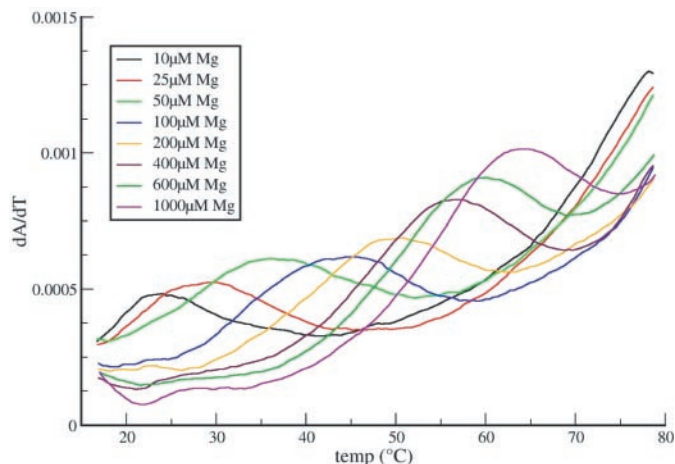


**Figure 3.** Superimposed first derivatives of melting curves of the kissing complex St1CCGACC/St2GGUCGG at different magnesium concentrations.

$Mg^{2+}$  is 29°C, compared with 40°C for the regular duplex (Figure 4). At higher magnesium concentrations, the opposite is true: at 1 mM  $Mg^{2+}$  the kissing complex melts at 63°C and the regular duplex at 57°C. The  $T_m/\log [\text{ion}]$  plots allow a precise comparison of the ion dependency of the kissing complex with that of the regular helix. The slope of the  $T_m/\log [Mg^{2+}]$  for the kissing loop is 16° and 8°C for the regular helix; the  $\Delta T_m/\log [Na^+]$  for the kissing loop is 26°C and for the regular duplex, 11°C (Table 4). At  $\sim 150 \mu M Mg^{2+}$  or 0.8 M  $Na^+$ , the kissing complex and the regular duplex are equally stable (Figure 4).

The number of magnesium ions bound per complex is revealed by plotting the melting temperature versus the logarithm of the  $Mg^{2+}$  concentration (27). For the kissing complex with the loop sequence AACCGACCA, at least two magnesium ions are bound, which agrees with the number of magnesium ions detected in the X-ray crystal structure (28). For monovalent sodium ions, our calculations suggest at least three ions bound in the kissing complex.

## DISCUSSION

While the prediction of the stability of RNA secondary structure elements is very precise, it is still not possible to accurately predict the stability of RNA tertiary structures, due to the lack of knowledge about the contribution of a single tertiary interaction to the overall stability of an RNA molecule. In order to address this issue, we measured thermodynamic parameters for WC type base pairs, which are involved in tertiary interactions. A set of four complementary hairpin loops derived from the HIV-1 DIS loop, which is a nine-base loop with six complementary bases, flanked by two adenines on the 5' end and one adenine on the 3' end, were designed. We compared the stability of the loop-loop kissing interaction between two such hairpin loops with the stability of a regular RNA helix of identical sequence with and without dangling adenines. The kissing complexes are more stable than the sequence equivalent regular duplexes for the four tested sequences by approximately  $-4$  kcal/mol when

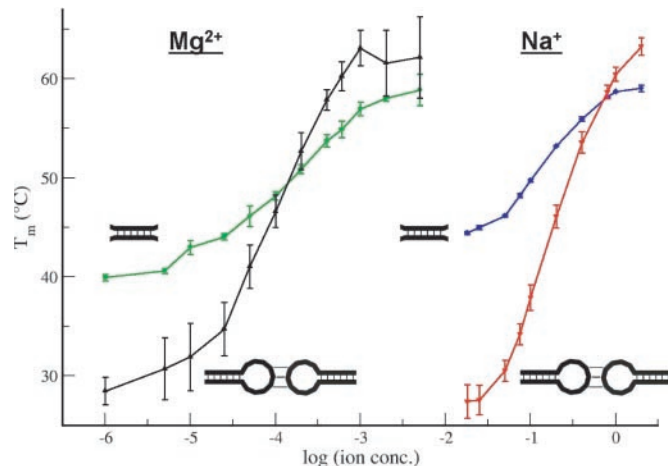


**Figure 4.** Influence of the ionic strength on the melting temperature of the kissing complex St1CCGACC/St2GGUCGG and of a regular RNA helix of identical sequence with dangling adenines. Left curves in black and green indicate the magnesium dependence of the kissing complex and the regular duplex, and the right curves in red and blue indicate sodium dependence of the kissing complex and the regular duplex, respectively. Duplexes at low magnesium concentrations (which always contain 18 mM sodium ions) are observed with  $T_m$  values below those for low sodium concentrations. A similar effect has been previously noted (37).

**Table 4.** Ionic stabilization of various melting transitions indicated as  $\Delta T_m/\log [\text{ion}]$  as published in this or previous works. Left column: as a function of  $[Mg^{2+}]$ ; right column as a function of  $[Na^+]$

Nucleic acid molecule	$\Delta T_m/\log [Mg^{2+}]$	$\Delta T_m/\log [Na^+]$	Refs
Kissing loop	16°C	26°C	This work
6 bp RNA + dangling As	8°C	11°C	This work
RNA I/RNA II wt/Ri	20–25°C		(27)
DNA/RNA long homopolymers		18°C	(33)
Long RNA duplexes		8–20°C	(38)
8 bp DNA or dumbbell		11°C	(35)
Hexameric RNA duplex	6°C	8°C	(34)
Octameric RNA duplex	5°C	8–10°C	
14Mer RNA duplex	4°C	13°C	
12 bp eubacterial Loop E	15°C		(34)
7 bp/5 bp pseudoknot	13°C		(36)
Hairpin with tetraloop		3.8°C	(39)

Experimental conditions as published: for homopolymers pH = 7.0; 8 bp DNA and dumbbell: 60  $\mu M$  DNA, 10 mM Na phosphate buffer pH = 7.0, 0.1 mM EDTA; RNA duplexes and loop E were 100  $\mu M$  RNA, 10 mM Na cacodylate pH = 7.0, 100 mM NaCl (for data on  $Mg^{2+}$ ); pseudoknot: 10 mM MOPS pH = 7.0, 100 mM KCl.

compared with helices without dangling adenines and approximately  $-1$  kcal/mol when compared with helices with dangling adenines. Since this difference is constant, it suggests that the nearest neighbor model is also valid for WC pairs in loop-loop interactions. This fact should enable the prediction of the stability of such loop-loop interactions by calculating the stability of regular helices and adding a constant stabilization factor, which might depend on the structural context of the interaction. For HIV DIS type loop-loop interactions, this benefit factor is  $-4$  kcal/mol at 1 M  $Na^+$ . Previous studies had shown that the purines flanking the base pairs contribute to the stability and to the association kinetics of the kissing complex (29).

The increased stability of the loop–loop interaction within the RNA dimer can be explained by the fact that the kissing interaction is sandwiched between two preformed hairpins further reducing its free energy by making favorable stacking interactions with the two adjacent hairpins. This can be clearly seen in the structure of the DIS complex (30). In its natural context, this structural motif further folds to form another even more stable complex by opening the stems and extending the base pairing on both sides of the kissing loop, the so-called extended complex (17,19). Since the kissing complex is so stable, the probability that the stems open more easily than the loop–loop interaction is increased, favoring extended complex formation over dissociation of the kissing complex.

Detailed thermodynamic parameters have already been reported for another type of kissing complex, namely, the complex between RNA I and RNA II, which are involved in the control of DNA replication of plasmid ColE1 (14,27). In this system, the loop consists of seven nucleotides and full complementarity of the two interacting loops is required to achieve full affinity. The stability of this type of loop–loop complex is heavily dependent on the identities of the first and last nucleotides and *in vivo* the RNA I/RNA II complex is stabilized by the RNA one modulator (ROM) protein (14).

### The kissing complex displays a stronger dependence on ion concentration than the regular RNA helix

Since the ionic strength has a significant impact on the stability of RNA structure, we tested the influence of magnesium and sodium concentrations on the melting temperature and found that the observations mentioned above are valid only in the presence of 1 M NaCl. At low salt concentrations, the regular helices are more stable than the kissing complex, while at high salt concentrations, the kissing complex is more stable than the regular helices. The salt concentration has a stronger influence on the stability of the kissing complex than on the regular helix, as reflected in the different slopes of the  $T_m/\log [\text{ion}]$  plots (Figure 4 and Table 4). The stability of the kissing complex and the regular helix are the same at the intersection of the  $T_m/\log [\text{ion}]$  plots.

The slope of the  $T_m$  versus  $\log [\text{ion}]$  plots indicates the difference in effective charge density for the transition between the two states. The melting temperature was expected to vary logarithmically with salt concentration, the slope depending theoretically on the change in the number of ions bound, on melting the structure. For any transition of charged polynucleotides, an increase in ionic strength of the solution affects the melting temperature such that the formation of the species with the higher effective charge density is favored. Then, in the low-salt approximation, the transition temperature will be a linear function of the logarithmic ion concentration with the form

$$T_m = T_m^0 - C \log [\text{ion}]$$

where  $T_m^0$  is the melting temperature in the absence of electrostatic effects and  $C$ , a constant related to the electrostatic contribution to free energy (31,32). The salt-dependence,  $dT_m/d\log [\text{ion}]$ , is linear over a range at low salt and then reaches saturation, corresponding to a lower slope, which is

due to complete charge neutralization of the polycations. Using a purely electrostatic model of ion binding and experimental data from secondary structure melting of nucleic acid homopolymers, parameters could be fitted to rationalize the behavior in the linear range and predict the salt-dependence with high accuracy. As will be shown further below, the parameter  $\Delta T_m/\Delta \log [\text{ion}]$  seems to be a sensitive indicator of RNA structural transitions.

For melting of long homopolymers in the presence of monovalents, the ionic stabilization is of 18°C per  $\log [\text{Na}^+]$  (33) as seen in Table 4. However, our data on short RNA helices shows a lower ionic stabilization of 11°C per  $\log [\text{Na}^+]$ . We have attempted a comparison between the values for the ionic stabilization obtained with our system and data from previously published melting experiments (Table 4). We estimate that slight differences in experimental conditions will have only a marginal influence. When plotting data from previous studies on short, regular RNA duplexes (34) we consistently found an ionic stabilization of about 10–11°C for 8mers. This value is independent of whether the helical stack contains dangling ends or not, whether the transition concerns RNA or DNA helices or even dumbbell-shaped DNA closed at both ends (35). For 6mer and 14mer duplexes, the respective ionic stabilization is 8° and 13°C per  $\log [\text{Na}^+]$ . Clearly, short duplexes do not satisfy the assumption of a helical rod of infinite length and therefore, behave differently. On the other hand, the kissing complex yields an ionic stabilization of 26°C per  $\log [\text{Na}^+]$ , showing a much stronger salt dependence of the tertiary interaction.

In the presence of  $\text{Mg}^{2+}$ , the ionic stabilization for 6, 8 and 14mers is typically 4–6°C at a relatively high concentration of 100  $\mu\text{M}$  RNA, when compared with 8°C for various 8mers with dangling ends (6 bp) at 3–9  $\mu\text{M}$  RNA. Again, the same base-pairing in the context of a tertiary interaction yields a significantly higher ionic stabilization of 16°C. Melting curves have also been measured for other RNA motifs that contain tertiary structure with a known dependence on  $\text{Mg}^{2+}$ . For the eubacterial loop E motif and for the T4 pseudoknot, the ionic stabilization is 15° and 13°C per  $\log [\text{Mg}^{2+}]$ , respectively (34,36). This is consistent with a higher salt-dependence of tertiary structure motifs. In fact, there is a large effective charge difference between separated hairpins in equilibrium with those coupled in the kissing complex, when compared with the two single strands in equilibrium with a helix. The structural preformation of the interacting hairpins is probably induced and stabilized by specific binding of a divalent ion as observed in solution (30) and in the crystal structures (28).

## CONCLUSIONS

A long-term goal of our project is to understand the rules that govern RNA folding at the tertiary structure level and to define the relationships between structure and stability. The analysis of the thermodynamic parameters of large RNA molecules is often too complex to derive the contribution of single structural motifs. We therefore began by analyzing a simple tertiary interaction composed of WC base pairs with respect to loop–loop interactions in order to demonstrate the feasibility of such

an approach. We further present free energy values suitable for the calculation of all loop-loop interactions of the HIV DIS type for different ionic conditions. Because of the linear correlation between the  $T_m$  and the ionic concentration, for a defined range of ion concentration, structural stabilities can be interpolated. The strong dependence of the stability of the tertiary loop-loop interactions in the kissing complexes concurs with the experimentally observed specific binding of divalent ions within the hairpin loops (28,30).

## SUPPLEMENTARY MATERIAL

Supplementary Material is available at NAR Online.

## ACKNOWLEDGEMENTS

We thank Peter Stadler and Ivo Hofacker for intensive discussions at the start of this project. The help of Paul Watson with the preparation of the manuscript is greatly appreciated. We thank all members of our laboratories for constant discussions and comments on the manuscript. This work was funded by the Austrian Science Fund, FWF, grant no. P16026 to RS. A.W. and E.W. thank the EU CARBONA (HPRN-CT-2002-00190) network for support.

## REFERENCES

- Chastain,M. and Tinoco,I.,Jr. (1991) Structural elements in RNA. *Prog. Nucleic Acid Res. Mol. Biol.*, **41**, 131–177.
- Batey,R.T., Rambo,R.P. and Doudna,J.A. (1999) Tertiary motifs in RNA structure and folding. *Angew. Chem. Int. Ed. Engl.*, **38**, 2326–2343.
- Conn,G.L. and Draper,D.E. (1998) RNA structure. *Curr. Opin. Struct. Biol.*, **8**, 278–285.
- Cate,J.H., Gooding,A.R., Podell,E., Zhou,K., Golden,B.L., Szewczak,A.A., Kundrot,C.E., Cech,T.R. and Doudna,J.A. (1996) RNA tertiary structure mediation by adenosine platforms. *Science*, **273**, 1696–1699.
- Brion,P. and Westhof,E. (1997) Hierarchy and dynamics of RNA folding. *Annu. Rev. Biophys. Biomol. Struct.*, **26**, 113–137.
- Tinoco,I.,Jr. and Bustamante,C. (1999) How RNA folds. *J. Mol. Biol.*, **293**, 271–281.
- Tinoco,I.,Jr., Borer,P.N., Dengler,B., Levin,M.D., Uhlenbeck,O.C., Crothers,D.M. and Bralla,J. (1973) Improved estimation of secondary structure in ribonucleic acids. *Nature New Biol.*, **246**, 40–41.
- Serra,M.J. and Turner,D.H. (1995) Predicting thermodynamic properties of RNA. *Methods Enzymol.*, **259**, 242–261.
- SantaLucia,J.,Jr. and Turner,D.H. (1997) Measuring the thermodynamics of RNA secondary structure formation. *Biopolymers*, **44**, 309–319.
- Mathews,D.H., Sabina,J., Zuker,M. and Turner,D.H. (1999) Expanded sequence dependence of thermodynamic parameters improves prediction of RNA secondary structure. *J. Mol. Biol.*, **288**, 911–940.
- Jaeger,J.A., SantaLucia,J.,Jr. and Tinoco,I.,Jr. (1993) Determination of RNA structure and thermodynamics. *Annu. Rev. Biochem.*, **62**, 255–287.
- Xia,T., SantaLucia,J.,Jr., Burkard,M.E., Kierzek,R., Schroeder,S.J., Jiao,X., Cox,C. and Turner,D.H. (1998) Thermodynamic parameters for an expanded nearest-neighbor model for formation of RNA duplexes with Watson–Crick base pairs. *Biochemistry*, **37**, 14719–14735.
- Leontis,N.B. and Westhof,E. (2001) Geometric nomenclature and classification of RNA base pairs. *RNA*, **7**, 499–512.
- Eguchi,Y. and Tomizawa,J. (1990) Complex formed by complementary RNA stem-loops and its stabilization by a protein: function of CoIE1 Rom protein. *Cell*, **60**, 199–209.
- Paillart,J.C., Marquet,R., Skripkin,E., Ehresmann,C. and Ehresmann,B. (1996) Dimerization of retroviral genomic RNAs: structural and functional implications. *Biochimie.*, **78**, 639–653.
- Wagner,C., Palacios,I., Jaeger,L., St Johnston,D., Ehresmann,B., Ehresmann,C. and Brunel,C. (2001) Dimerization of the 3'UTR of bicoid mRNA involves a two-step mechanism. *J. Mol. Biol.*, **313**, 511–524.
- Laughrea,M. and Jette,L. (1996) Kissing-loop model of HIV-1 genome dimerization: HIV-1 RNAs can assume alternative dimeric forms, and all sequences upstream or downstream of hairpin 248–271 are dispensable for dimer formation. *Biochemistry*, **35**, 1589–1598.
- Brunel,C., Marquet,R., Romby,P. and Ehresmann,C. (2002) RNA loop-loop interactions as dynamic functional motifs. *Biochimie.*, **84**, 925–944.
- Windbichler,N., Werner,M. and Schroeder,R. (2003) Kissing complex-mediated dimerisation of HIV-1 RNA: coupling extended duplex formation to ribozyme cleavage. *Nucleic Acids Res.*, **31**, 6419–6427.
- Laing,L.G., Gluick,T.C. and Draper,D.E. (1994) Stabilization of RNA structure by Mg ions. Specific and non-specific effects. *J. Mol. Biol.*, **237**, 577–587.
- Heilman-Miller,S.L., Thirumalai,D. and Woodson,S.A. (2001) Role of counterion condensation in folding of the Tetrahymena ribozyme. I. Equilibrium stabilization by cations. *J. Mol. Biol.*, **306**, 1157–1166.
- Banerjee,A.R., Jaeger,J.A. and Turner,D.H. (1993) Thermal unfolding of a group I ribozyme: the low-temperature transition is primarily disruption of tertiary structure. *Biochemistry*, **32**, 153–163.
- Tanner,M. and Cech,T. (1996) Activity and thermostability of the small self-splicing group I intron in the pre-tRNA(Ile) of the purple bacterium *Azoarcus*. *RNA*, **2**, 74–83.
- Brion,P., Michel,F., Schroeder,R. and Westhof,E. (1999) Analysis of the cooperative thermal unfolding of the td intron of bacteriophage T4. *Nucleic Acids Res.*, **27**, 2494–2502.
- Tinoco,I.,Jr. and Schmitz,M. (2000) Thermodynamics of formation of secondary structure in nucleic acids. In Cera,E.D. (ed.), *Thermodynamics in Biology*. Oxford University Press, Oxford, pp. 131–176.
- Hofacker,I.L. (2003) Vienna RNA secondary structure server. *Nucleic Acids Res.*, **31**, 3429–3431.
- Gregorian,R.S.,Jr. and Crothers,D.M. (1995) Determinants of RNA hairpin loop-loop complex stability. *J. Mol. Biol.*, **248**, 968–984.
- Ennifar,E., Walter,P., Ehresmann,B. and Ehresmann,C. (2001) Crystal structures of coaxially stacked kissing complexes of the HIV-1 RNA dimerization initiation site. *Nature Struct. Biol.*, **8**, 1064–1068.
- Paillart,J.C., Berthoux,L., Ottmann,M., Darlix,J.L., Marquet,R., Ehresmann,B. and Ehresmann,C. (1996) A dual role of the putative RNA dimerization initiation site of human immunodeficiency virus type 1 in genomic RNA packaging and proviral DNA synthesis. *J. Virol.*, **70**, 8348–8354.
- Jossinet,F., Paillart,J.C., Westhof,E., Hermann,T., Skripkin,E., Lodmell,J.S., Ehresmann,C., Ehresmann,B. and Marquet,R. (1999) Dimerization of HIV-1 genomic RNA of subtypes A and B: RNA loop structure and magnesium binding. *RNA*, **5**, 1222–1234.
- Record,M.T.,Jr. (1967) Electrostatic effects on polynucleotide transitions. II. Behavior of titrated systems. *Biopolymers*, **5**, 993–1008.
- Cantor,C.R. and Schimmel,P.R. (1980) *Biophysical Chemistry: The Behavior of Biological Macromolecules*. W.H. Freeman, San Francisco.
- Guschlbauer,W. (1976) *Nucleic Acid Structures*. Springer, NY.
- Serra,M.J., Baird,J.D., Dale,T., Fey,B.L., Retatagos,K. and Westhof,E. (2002) Effects of magnesium ions on the stabilization of RNA oligomers of defined structures. *RNA*, **8**, 307–323.
- Rentzperis,D., Ho,J. and Marky,L.A. (1993) Contribution of loops and nicks to the formation of DNA dumbbells: melting behavior and ligand binding. *Biochemistry*, **32**, 2564–2572.
- Nixon,P.L. and Giedroc,D.P. (1998) Equilibrium unfolding (folding) pathway of a model H-type pseudoknotted RNA: the role of magnesium ions in stability. *Biochemistry*, **37**, 16116–16129.
- Heerschap,A., Walters,J.A.L.I. and Hilbers,C.W. (1985) Interactions of some naturally occurring cations with phenylalanine and initiator tRNA from yeast as reflected by their thermal stability. *Biophys. Chem.*, **22**, 205–217.
- Steger,G., Muller,H. and Riesner,D. (1980) Helix-coil transitions in double-stranded viral RNA. Fine resolution melting and ionic strength dependence. *Biochim. Biophys. Acta*, **606**, 274–284.
- Antao,V.P., Lai,S.Y. and Tinoco,I.,Jr. (1991) A thermodynamic study of unusually stable RNA and DNA hairpins. *Nucleic Acids Res.*, **19**, 5901–5905.